Bio-sensing with butterfly wings: naturally occurring nano-structures for SERS-based malaria parasite detection

Natalie L. Garrett[1,2], Ryo Sekine[1,3], Matthew W.A. Dixon[4], Leann Tilley[4], Keith R. Bambery[5], Bayden R. Wood[1]

1. Centre for Biospectroscopy, School of Chemistry, Monash University, 3800, Victoria, Australia.
2. School of Physics, University of Exeter, Stocker Road, Exeter, Devon, EX4 4QL.
3. Centre for Environmental Risk Assessment and Remediation, University of South Australia, Mawson Lakes, South Australia 5095, Australia.
4. Department of Biochemistry and Molecular Biology, Bio21 Institute, The University of Melbourne, Victoria 3010, Australia.
5. Australian Synchrotron, 800 Blackburn Rd Clayton, Victoria 3168, Australia.

ABSTRACT Surface enhanced Raman scattering (SERS) is a powerful tool with great potential to provide improved bio-sensing capabilities. The current 'gold-standard' method for diagnosis of malaria involves visual inspection of blood smears using light microscopy, which is time consuming and can prevent early diagnosis of the disease. We present a novel surface-enhanced Raman spectroscopy substrate based on gold-coated butterfly wings, which enabled detection of malarial hemozoin pigment within lysed blood samples containing 0.005 % and 0.0005 % infected red blood cells.

KEYWORDS Malaria, blood, Raman, SERS

Malaria the disease is caused by infection with the Apicomplexan parasite, *Plasmodium sp.*. Worldwide hundreds of millions of people are infected annually, resulting in 0.6-1.2 million deaths[1]. With early detection and prompt treatment the disease is curable, but the limitations of microscopic examination of stained blood smears (the current 'gold-standard' diagnosis method) can inhibit timely diagnosis. Time-consuming manual microscopic examination of stained blood films suffers from human subjectivity, leading to false negative diagnoses, especially for patients in the earliest stages of infection where parasite numbers are low[2]. Although, Tip-enhanced Raman Scattering (TERS) has recently been used to detect the parasite derived hemoglobin breakdown product hemozoin, within a single sectioned red blood cell (RBC)[3] and there is a report[4] on using surface-enhanced Raman scattering (SERS) to detect β-hematin (synthetic hemozoin), the potential for SERS to detect hemozoin in bulk malaria parasite-infected blood samples has not yet been exploited. Here we present an effective and novel method requiring minimal sample preparation, using gold-coated butterfly wings as a SERS platform for rapid analysis of the ring-stage parasites. This method may provide a basis for faster, less user-biased diagnosis methods facilitating timely and effective treatment of the disease.

The most lethal strain of malaria is caused by the parasite *Plasmodium falciparum*, which is transmitted to humans via a bite from an infected female *Anopheles* mosquito. The parasite has a complex lifecycle within the human host, part of which involves invasion of RBCs to undergo asexual reproduction for a period of 48 hours. During this erythrocytic phase, the parasite digests up to 75 % of the cell's hemoglobin (by dry weight[4]) by a cascade of enzymatic cleavage events resulting in peptides and the subsequent release of toxic free heme as a by-product[6]. The parasite initiates a detoxification process, converting free heme into ferriprotoporphyrin, which precipitates inside the digestive vacuole as crystals of the non-toxic, insoluble hemozoin.

During the 48-hour erythrocytic cycle the ring-stage parasites mature into trophozoites, changing the surface properties of the cells, which causes these cells to adhere to blood vessels[5]. Thus, since samples of infected blood taken from the body's peripheral circulation are used for diagnosis, only cells from the earlier time points of the parasite's 48-hour erythrocytic phase will be present in a diagnostic sample. An alternative malaria diagnosis technique for detection of these circulating ring stage parasites would help with the early and pre-patent identification of infection allowing prompt treatment. In laboratory settings, using optical microscopy only between 75 % - 90 % of infected blood samples are correctly identified as being infected, but this can be as poor as 50 % in the field[6]. Most routine diagnostic laboratories are able to detect infection at levels of 0.01% of the total red blood cell count (approximately 500 parasites per μL). Automated flow cytometry of blood samples provides sensitivities that vary dramatically depending on the immunity of the patient[7]. Rapid diagnostic testing (RDT) is an alternative technique, which employs antibody-antigen binding on dipsticks, but this only provides a qualitative measure of infection. There are currently 20 different RDTs available on the market, with widely variable sensitivity and specificity[6]. Diagnostic methods based on detecting hemozoin are challenging as mature stage parasites, which contain the highest levels of hemozoin, are not present in the circulation. As an alternative the level of hemozoin in monocytes (that have been ingested infected RBCs) has been investigated as a potential diagnostic indicator of the disease[7], but was not sufficiently reliable for non-immune patients. The ideal diagnosis method would be able to rapidly detect low levels of early stage parasites in blood from patients and would require little technical training in the practitioner.

Laser Raman spectroscopy is a powerful alternative technique to optical microscopy which can be used to probe the hemozoin content of RBCs. Although spontaneous Raman scattering is a weak process with typical scattering cross sections of ~ 10^{-30} cm^2 per molecule, Raman

acoustic levitation spectroscopy has been successfully used to detect hemozoin within a 5 μL droplet containing live infected RBCs, of which 6 % were infected[8]. In order to adapt this technique for rapid spectral acquisition in a diagnostic setting with typically low levels of parasitemia (i.e. ~ 0.05% of the total number of RBCs in the sample volume exhibiting parasitic infection), it is necessary to boost the weak Raman signal, without incurring photo-induced damage in the sample from simply increasing the laser power. Resonance Raman spectroscopy is one such method, whereby the incident laser light wavelength is chosen to closely match an electronic transition of the molecule being probed, resulting in an enhanced signal[9]. Even stronger enhancements are possible with SERS, wherein electromagnetic and chemical enhancements of the Raman signal are obtained when metallic nano-structures are brought within close proximity of the molecules of interest [10,11].

With typical SERS substrates, the intensity of the Raman-scattered light has been shown to be enhanced relative to spontaneous Raman scattering typically by factors of between 10^6 and 10^9 [12]. Much work has been undertaken to manufacture precise SERS platforms of nano-structures, for instance: silver nanohexagonal columns[13]; on metals can be expensive and time consuming, leading to inefficient experiments where each platform is used only once. To reduce costs and improve SERS enhancements, many scientists are now looking to naturally occurring nano-structures for inspiration, such as the nipple array anti-reflective coatings on cicada wings[14] and the naturally-occurring nano-structures that occur on butterfly wings[10,15]. Previous work has demonstrated that the purple and blue regions on the wings of the brightly colored *Graphium weiskei* butterfly (Fig. 1) exhibit nano-conical structures composed of the structural protein chitin that can be used to make biologically compatible SERS platforms (Fig. 2)[10]. To date, the promising SERS enhancements yielded by such naturally occurring structures have not been exploited beyond proof-of-concept experiments.

In this Letter, we experimentally demonstrate that SERS platforms made from gold-coated *G. weiskei* wings can be used to detect hemozoin crystals in samples of lysed blood containing 0.0005% (Fig. 3 A) and 0.005% (Fig. 3 B) early ring-stage *P. falciparum*-infected RBCs. Using SERS substrates made from gold-coated wings of *G. weiskei* butterflies, as illustrated in Fig. 1, we detected the strong ν_4 pyrrole in-phase breathing vibration Raman shift at 1375 cm^{-1} within malarial hemozoin pigment in lysate from RBCs infected with the malaria parasite *P. falciparum*. Additionally, a second characteristic marker of hemozoin, ν_{11}, located at ~1569 cm^{-1}, as reported by Brémard *et al.*[16], was also detected within the infected samples, but not in the uninfected lysate. The uninfected lysate is a mixture of dried hemoglobin and membrane structures and consequently the spectrum is dominated by overlapping heme and lipid bands. We found no competing spectral features from the chitinous wing surface prior to coating the substrates with lysate, a finding that is consistent with our previous observations using this thickness of gold coating[10]. Furthermore, hemozoin has a much larger Raman cross-section compared to chitin due to the symmetry and chromophoric nature of the former, which is further increased during a SERS measurement.

Due to the inhomogeneous nature of the sample, the SERS spectra obtained were taken as averages over 5 spectra, each obtained at a separate location on the sample, in order to account for regional variations. Acquisition times were kept as short as possible, to minimize heating that could cause sample damage. The SERS spectra of 0.0005% and 0.005% *P. falciparum*-infected RBC lysate obtained in Figs. 3 A and B exhibit several bands that are enhanced relative to the spontaneous Raman spectrum of hemozoin in Fig. 3 D, namely 1570 cm^{-1}, 1376 cm^{-1}, 798 cm^{-1} and 679 cm^{-1}, which are associated with totally symmetric A_{1g} modes. These SERS spectra also showed contributions from methine C-H deformation ν_{13}

and at 1219 and 1221 cm^{-1} and the ν_{42} amide III and 1240 and 1238 cm^{-1} for 0.005% and 0.0005% *P. falciparum*-infected RBC lysate, respectively.

Interestingly, when the lysate-coated wings were examined with scanning electron microscopy, there was no evidence of the typical needle-like hemozoin crystals (~ 2 μm long) [17] reported within the digestive vacuoles of mature *P. falciparum*. Wing samples that were not exposed to lysate were also imaged to provide a control sample for comparison, as shown in Fig. 2. C and D. The only discernible crystals on the lysate-coated sample, as illustrated in Fig. 2. A, were determined to be sodium chloride using energy-dispersive x-ray spectroscopy. However, a layer of deposit was discovered to exist surrounding the base of the conical features on the wing, as can be made out in Fig. 2. B. We have hypothesized from these findings that the crystals present within such early ring-stage parasites are on the nano-scale and as such, are difficult to locate in the milieu of dried hemoglobin and membrane structures. This finding is not without precedent, as previous work has determined that hemozoin crystals from early-stage rings are typically much smaller than those within mature parasite digestive vacuoles [18].

Assuming that the nano-scale hemozoin crystals exist in the layer of deposit surrounding the base of the conical wing protrusions, and given that we see no significant evidence of hemoglobin contributions to the SERS spectra, this offers a clue as to the origin of the enhancement. If, as suggested in the SEM images, the hemozoin crystals aggregate at the base of the conical nano-structures, this could lead to enhancement of these high-spin ferric hemes[19] in addition to surface enhancement effects, but not of hemoglobin markers (such as the ν_{10} oxygenated peak at 1605 cm^{-1} and deoxygenated peak at 1640 cm^{-1} [20]).

Given that the substrate surface is not functionalized, the deposition of hemozoin from the lysate is random. Moreover, the hemozoin crystals tend to aggregate in solution. These two factors make

locating a ‘hot-spot’ on the substrate at concentrations below 0.0005% prohibitively time-consuming. However, in SERS spectra acquired from regions of the substrate where hemozoin is present, the variation in the relative peak height for the ν_4 pyrrole in-phase breathing vibration characteristic of hemozoin when compared to ν_{10} was generally found to be less than 5%. The limitation in this approach is the time required to record an image sufficiently large enough to detect the “hot spots” and the fact that the relative peak enhancement is not an indicator of hemozoin concentration.

The origin of the SERS enhancement in protruding substrates such as the array of nano-cones in these substrates, arises from a complex interplay between every surface within the considerable near-field evanescent modes[21]. Modeling the local plasmonic field of such an array is rendered prohibitively complex since to the quasi-periodic spacing and non-uniform cone length and orientation makes the sample effectively random. Previous investigations into the origin of the Raman enhancement experienced in ‘v-grooves’ has indicated that surface plasmons are not the major contributing factor to Raman enhancement within the cavity of micron-sized gold-coated pyramidal pits[22]. In fact, with such structures it was discovered that classical electromagnetic Raman enhancement of E^4 arose from near-field diffraction effects. Given that the dimensions of the v-shaped bases of the nano-cones found on the *G. weiskei* substrates are on the same scale as those modeled by Mechler *et al.*, it is likely that near-field diffraction has an effect on the wing-based samples as well. However with these wing-based substrates it is a combination of inter-cone spacing, metal thicknesses on the edge of the cones relative to the spaces between the cones, that combines to produce a substrate capable of yielding SERS enhancement factors of up to 1.9×10^6 when coated with gold [10].

These wing-based substrates are relatively inexpensive and simple to produce, but it is feasible that a form of large-scale replication of the wings’ surface features would be required for industrial-scale production. Since laboratory research doesn’t require large batch

production of such substrates, lithographic methods have still not been adopted by many researchers in the field, who instead use insect wings as they are found naturally [23]. However, Stoddart *et al.* have developed a low-cost, high-resolution nano-imprinting technique using UV and heat-based curing systems for generating polymer-based nano-structured surfaces on optical fibres, replicating the structural features found on cicada wings for SERS substrates[24]. Additionally, three-dimensional hierarchical structures of butterfly wing scales have been produced in copper replicas using selective surface functionalization and subsequent electroless deposition, which have generated significant SERS enhancement[25,26]. Even though the structure of these cicada wings and butterfly wing scales are very different to the conical structures exhibited by *G. weiskei*, these nanostructure replication methods could be applied to *G. weiskei* wings for future larger-scale applications of these substrates to bio-sensing.

In conclusion, we have been able to identify key characteristic spectral markers of the malarial pigment hemozoin within lysate from infected RBC samples exhibiting early-ring stage parasitemia levels of between 0.0005% and 0.005%. This represents a major advance in spectroscopic detection of early stage malarial infection and leads us closer to the development of SERS-based diagnosis methods. More broadly, our work additionally demonstrates the suitability of these substrates for bio-medical applications of SERS, with potential use beyond the field of malaria diagnosis.

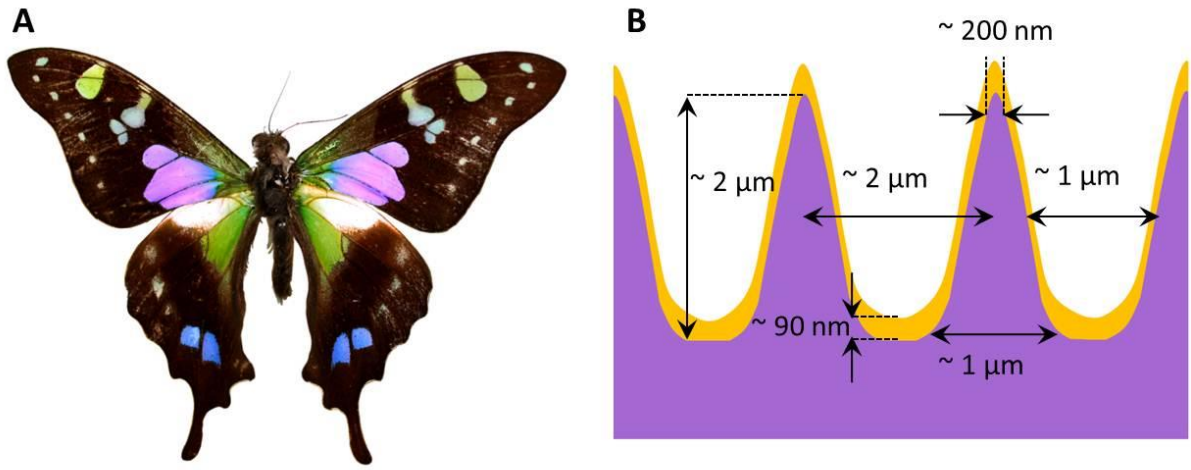

Figure 1. *Graphium weiskei* butterfly wings as SERS substrates. A: *G. weiskei* butterfly sample. B: Schematic cross-sectional view of a gold-coated wing. Typical chitinous conical protrusion dimensions and spacing are based on visual investigation of SEM images.

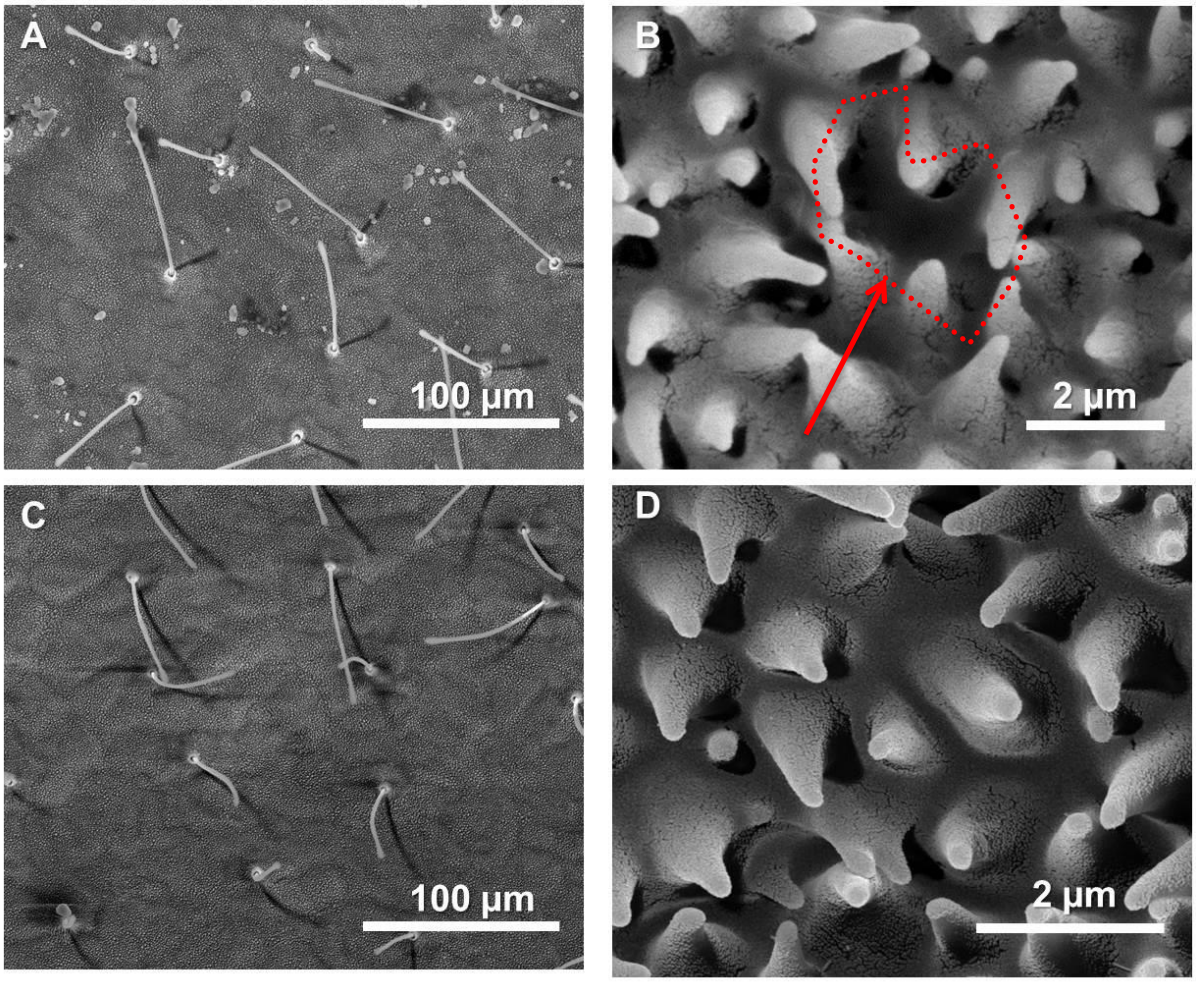

Figure 2. SEM images of chitinous nano-structured conical arrays found on the wings of the *G. weiskei* butterfly. A & B: SEM images acquired after deposition with *P. falciparum*-infected RBC lysate. The red boundary indicates an example of where a lysate has locally deposited and the surface darkened compared to areas without the deposit. C & D: control butterfly wings without lysate deposition.

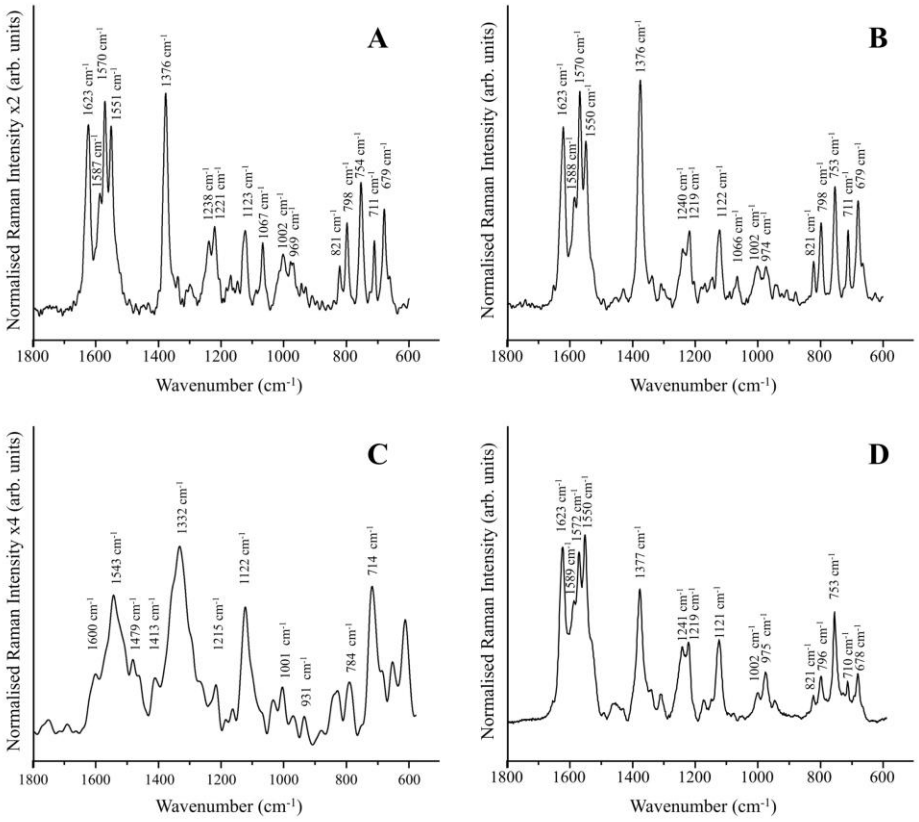

Fig. 3 A – C: SERS spectra of 0.0005%, 0.005% and 0% (control) malarial-infected RBC lysate, respectively. D: Conventional Raman spectrum of hemozoin at 785 nm.

Methods

All glassware was cleaned with aqua regia (a mixture of concentrated hydrochloric acid and concentrated nitric acid in a 3 : 1 ratio by volume) and rinsed exhaustively in Millipore water prior to use. Sections of *G. weiskei* wings were fixed to glass microscope slides using a UV-curing adhesive (Norland optical adhesive, Cranbury, USA) before being coated with gold films (99.999% purity, GMBH) within a vacuum thermal evaporator at a deposition rate of 0.5 nm s^{-1}. A quartz microbalance crystal was used to monitor the thickness of the deposited film, which was later verified using atomic force microscopy (Ntegra NT-MDT, Russia),

which was 100 nm. Since the wing surface is not flat, this thickness is a maximum rather than an absolute measure of the gold film thickness on the wing. At the edges of regions of the wing that were obscured during gold deposition, typical film thickness was determined to be approximately 90 nm

P. falciparum was cultured as previously described [27]. Briefly, parasite-infected RBCs were cultured in O+ RBCs (Australian Red Cross blood service), in RPMI-GlutaMAX$^{(TM)}$-HEPES (Invitrogen) supplemented with 5% v/v human serum (Australian Red Cross blood service), 0.25% w/v AlbuMAX II (Invitrogen), 0.58 mg/L gentamycin (Invitrogen) and 10 mM glucose. Parasite-infected RBCs were maintained at 37^{o}C in a low oxygen environment (5% CO_2, 1% O_2 in N_2). Ring stage parasites (0-12 h post invasion) were prepared from culture by two sorbitol synchronization steps to generate a ~10 h window of early stage parasites[28].

Ring-stage infected RBC stocks were added to washed uninfected RBCs to yield a percentage of infected cells of 0.05% or 0.005%. These stocks were spun down and further diluted in distilled water to induce lysis, yielding a final effective percentage of infected RBCs of 0.005% and 0.0005%. Aliquots of lysate were deposited onto gold-coated wing samples and dried in air prior to spectral acquisition and SEM imaging (FEI Quanta 3D FEG in SE mode).

Raman imaging of parasite lysates was performed on a WITec confocal CRM alpha 300 Raman microscope. The spectrometer was equipped with an air–cooled solid state laser operating at 785 nm and a back illuminated CCD detector, which was cooled to –65°C. The laser was coupled to a microscope via a single mode optical fiber with a diameter of 50 μm and the typical power at the sample was 5 μW. The scattered radiation was focused onto a multi–mode fiber (50 μm diameter) and a monochromator. The integration time for a single spectrum was 0.3 s with a spectral resolution of 3 cm^{-1}. The monochromator of the spectrometer was calibrated using the Raman scattering line produced by a silicon plate

(520.7 cm^{-1}). Baseline correction was carried out using OPUS 6.0 with spectra averaged over 5 acquisitions.

References

1 World Health Organisation, *World Malaria Report 2012*, 2012.

2 M. L. Wilson, *Clin. Infect. Dis.* , 2012, **54** , 1637–1641.

3 B. R. Wood, E. Bailo, M. A. Khiavi, L. Tilley, S. Deed, T. Deckert-Gaudig, D. McNaughton and V. Deckert, *Nano Lett.*, 2011, **11**, 1868–1873.

4 S. Francis, *Annu. Rev. …*, 1997, 97–123.

5 M. Ho and N. J. White, *Am. J. Physiol. - Cell Physiol.* , 1999, **276** , C1231–C1242.

6 M. L. Wilson, *Clin. Infect. Dis.*, 2012, **54**, 1637–41.

7 M. P. Grobusch, T. Hänscheid, B. Krämer, J. Neukammer, J. May, J. Seybold, J. F. J. Kun and N. Suttorp, *Cytometry B. Clin. Cytom.*, 2003, **55**, 46–51.

8 L. Puskar, R. Tuckermann, T. Frosch, J. Popp, V. Ly, D. McNaughton and B. R. Wood, *Lab Chip*, 2007, **7**, 1125–1131.

9 B. R. Wood and D. McNaughton, *Expert Rev. Proteomics*, 2006, **3**, 525–44.

10 N. L. Garrett, P. Vukusic, F. Ogrin, E. Sirotkin, C. P. Winlove and J. Moger, *J. Biophotonics*, 2009, **2**, 157–166.

11 J. R. Lombardi and R. L. Birke, *J. Phys. Chem. C*, 2008, **112**, 5605–5617.

12 E. C. Le Ru, E. Blackie, M. Meyer and P. G. Etchegoin, 2007, 13794–13803.

13 Y. S. Yamamoto, K. Hasegawa, Y. Hasegawa, N. Takahashi, Y. Kitahama, S. Fukuoka, N. Murase, Y. Baba, Y. Ozaki and T. Itoh, *Phys. Chem. Chem. Phys.*, 2013, **15**, 14611–14615.

14 P. R. Stoddart, P. J. Cadusch, T. M. Boyce, R. M. Erasmus and J. D. Comins, *Nanotechnology*, 2006, **17**, 680–686.

15 J. Moger, N. L. Cornes and P. Vukusic, eds. J. Popp and G. von Bally, SPIE, Munich, 2007, vol. 6633.

16 C. Brémard, P. Kowalewski, J. C. Merlin and S. Moreau, *J. Raman Spectrosc.*, 1992, **23**, 325–333.

17 G. S. Noland, N. Briones and D. J. Sullivan Jr., *Mol. Biochem. Parasitol.*, 2003, **130**, 91–99.

18 N. Abu Bakar, N. Klonis, E. Hanssen, C. Chan and L. Tilley, *J. Cell Sci.*, 2010, **123**, 441–50.

19 R. Puntharod, G. T. Webster, M. Asghari-Khiavi, K. R. Bambery, F. Safinejad, S. Rivadehi, S. J. Langford, K. J. Haller and B. R. Wood, *J. Phys. Chem. B*, 2010, 114, 12104–15.

20 I. P. Torres Filho, J. Terner, R. N. Pittman, E. Proffitt and K. R. Ward, *J. Appl. Physiol.* , **104** , 1809–1817.

21 Q. Hao, Y. Zeng, B. Juluri, X. Wang and B. Kiraly, *ACS ...*, 2011, 5472–5477.

22 M. Mechler, S. V Kukhlevsky, A. Mechler and D. McNaughton, *Phys. Chem. Chem. Phys.*, 2011, **13**, 20772–8.

23 L. Guo, C. X. Zhang, L. Deng, G. X. Zhang, H. J. Xu and X. M. Sun, *J. Appl. Phys.*, 2014, **115**, 213101.

24 G. Kostovski, D. J. White, a Mitchell, M. W. Austin and P. R. Stoddart, *Biosens. Bioelectron.*, 2009, **24**, 1531–5.

25 Y. Tan, J. Gu, X. Zang, W. Xu, K. Shi, L. Xu and D. Zhang, *Angew. Chemie*, 2011, **123**, 8457–8461.

26 Y. Tan, J. Gu, L. Xu, X. Zang, D. Liu, W. Zhang, Q. Liu, S. Zhu, H. Su, C. Feng, G. Fan and D. Zhang, *Adv. Funct. Mater.*, 2012, **22**, 1578–1585.

27 M. W. A. Dixon, S. Kenny, P. J. McMillan, E. Hanssen, K. R. Trenholme, D. L. Gardiner and L. Tilley, *Mol. Microbiol.*, 2011, **81**, 982–993.

28 C. Lambros and J. P. Vanderberg, *J. Parasitol.*, 1979, **65**, 418–420.